Kinetics studies of the reversible partial decomposition reaction in $Mg(BH_4)_2$

Olena Zavorotynska, Stefano Deledda, Bjørn C. Hauback

Physics Department, Institute for Energy Technology, P.O. Box 40, NO-2027, Kjeller, Norway

E-Mail: olena.zavorotynska@ife.no; stefano.deledda@ife.no; bjorn.hauback@ife.no

Abstract

Magnesium borohydride $Mg(BH_4)_2$ is a promising candidate for hydrogen storage due to its high hydrogen content and theoretically predicted low decomposition temperature. Hydrogenation of the completely decomposed $Mg(BH_4)_2$ requires high temperature, high H_2 pressure and long reaction time. However, the partially decomposed compound can be rehydrogenated in much milder conditions. In this work, we study the reversible intermediate decomposition reaction in $Mg(BH_4)_2$. Gravimetric and volumetric measurements have shown that $Mg(BH_4)_2$ released up to 6.8 wt% H_2 below 285 °C with the formation of amorphous MgB_xH_y intermediate(s), as found by infrared spectroscopic analysis. No crystalline decomposition reaction products were detected by powder X-ray diffraction. Rehydrogenation at 260-280 °C yielded 2.5 wt% uptake and the formation of crystalline $Mg(BH_4)_2$. Kinetics modeling suggested that the decomposition is a complex process with possibly several reactions which are limited mostly by diffusion. The rehydrogenation reaction was governed by the Johns-Mehl-Avrami model with the nucleation at a constant rate and diffusion-controlled growth mechanism.

Introduction

Storage of hydrogen has been the bottleneck for the hydrogen economy for decades. Present-day commercially-available solutions such as liquid and pressurized hydrogen tanks suffer from considerable energy losses, expensive storage tanks, and safety risks [1]. Therefore alternative solutions such as storage of chemically-bonded hydrogen in hydrides have been

Postprint.
Original in International Journal of Hydrogen Energy, Volume 41, Issue 23, 22 June 2016, Pages 9885–9892

explored [1-4] and commercialized [5, 6]. A hydrogen storage system is subject to a wide range of requirements. Among them are high hydrogen content, low temperature (*T*) and pressure (*p*) working conditions, fast kinetics of hydrogen desorption and absorption, and high purity of thereleased and re-absorptioned hydrogen [7]. Complex hydrides, such as magnesium borohydride ($Mg(BH_4)_2$), contain hydrogen-rich anions and have high gravimetric and volumetric hydrogen densities suitable even for the capacity-demanding on-board hydrogen storage applications. It is also predicted that $Mg(BH_4)_2$ has favorable thermodynamics which would allow hydrogen desorption at a temperature below 100 °C [8-10]. Experiments show, however, that the decomposition of $Mg(BH_4)_2$ requires at least 200 °C [11-20]. This has been partially attributed to slow kinetics and intermediate decomposition phases [21]. The studies on $Mg(BH_4)_2$ decomposition indeed suggest that the reaction pathway has several steps, and the nature of the intermediates is still debated [11-20]. Rehydrogenation of the completely decomposed $Mg(BH_4)_2$ requires high *T* and *p* [22, 23], but if the dehydrogenation reaction is stopped below 300 °C, partial rehydrogenation [11, 16-19, 24] and even cycling of about 2 wt% H_2 for 3 cycles was shown to be feasible [19]. It has been suggested that $Mg(B_3H_8)_2$ is formed in this incomplete decomposition reaction, yielding only 2.8 wt% of H_2 [11]. However, other studies indicate that below 300 °C the amount of desorbed H_2 can reach higher values [18]. In this work we report the findings on the reversible partial decomposition reaction in $Mg(BH_4)_2$ at different *T* and *p*. The amounts desorbed with a H_2 back pressure, in vacuum, and in Ar flow were evaluated. The desorption and absorption isotherms were modeled according to several solid-state reaction equations in order to determine the reaction kinetics and rate-limiting steps [25, 26].

Materials and Methods

Materials

All procedures were carried out in a glove box under a continuously purified Ar atmosphere (O_2, H_2O < 1 ppm) if not mentioned otherwise.

Commercial γ-$Mg(BH_4)_2$ (Sigma-Aldrich, 95%) was used. Powder X-ray diffraction (PXD) analysis showed that the crystalline fraction of this batch consisted of γ-$Mg(BH_4)_2$ [19].

Postprint.
Original in International Journal of Hydrogen Energy, Volume 41, Issue 23, 22 June 2016, Pages 9885–9892

Experimental methods

Hydrogen desorption and absorption isotherms (see Table 1 for details) were obtained in a calibrated Sieverts-type apparatus built in-house, equipped with a Pt100 class B temperature sensor and 870B Micro-Baraton® pressure transducer. Before all the measurements, the sample was kept in dynamic vacuum at room temperature (R*T*) for several hours. For the desorption measurements in vacuum, the samples were heated to the required temperature in static vacuum. For the desorption measurements in H_2 (p_0 = 2.5 bar), the samples were heated to the required temperature at a back pressure of 50 bar H_2 to hinder H_2 desorption during heating. At isothermal conditions, the pressure was reduced to 2.5 bar H_2. The samples decomposed at 262.5 and 284.4 °C were rehydrogenated. For the absorption measurements, the required hydrogen absorption pressure was set at R*T* and then the samples were heated to the required temperature. In case of absorption at 248.6 °C the *T* was raised to 260.3 °C due to the slow absorption kinetics. The amount of desorbed/absorbed hydrogen was determined from the pressure changes in the closed calibrated volume. The temperature variation during the isothermal steps was within ±2.5 °C during the first 30 min and not more than ±0.5 °C for the remaining duration of the measurement. In most cases the desorption reaction at the final stages was very slow and was stopped before completion. The details of the desorption and absorption measurements are listed in Table 1.

Approximately 0.3 g of sample was used in the desorption measurements. The total volume of the volumetric set-ups was 180 and 330 ml. The Δp during the desorption in static vacuum (p_0 = 0) was 0.5 bar at 221 °C, and between 0.8 and 1.3 bar at the higher *T*. For the desorption at H_2 backpressure (p_0 = 2.5 bar) Δp was between 0.2 and 0.6 bar. About 0.15 g was used for the absorption measurements with the total volume of the system of ca. 30 ml. The experimental conditions and results are detailed in Table1.

Table 1. Experimental conditions and results of the decomposition and rehydrogenation reactions. The average temperatures are given with estimated standard deviations.

$\bar{T}_{iso}$, °C	$p_{start} - p_{end}$, bar	measurement time *t*, h	amount H_2, Δwt%

Decomposition			
221.4 ± 0.9	0.0-0.5	95	3.6
262.5 ± 0.2	0.0-0.8	28	5.9
272.0 ± 0.1	0.0-0.9	29	6.5
284.4 ± 0.7	0.0-1.3	70	6.8
223.1 ± 0.2	2.7-2.9	70	1.3
265.5 ± 0.3	2.6-3.2	44	4.4
284.3 ± 0.5	2.6-3.1	70	3.6
265.1 ± 0.7	Ar flow 50 ml/min	10	8.1
285.1 ± 0.7	Ar flow 50 ml/min	6	9.1
Rehydrogenation			
279.8 ± 0.1	125.6 – 123.9	21	2.5
260.3 ± 0.1	122.9 – 120.7	11	2.5
248.6 ± 0.1	99.2 – 98.9	42	0.25

Synchrotron powder X-ray diffraction (SR-PXD) data were collected at the Swiss-Norwegian Beam Line (station BM01A) at the European Synchrotron Radiation Facility (ESRF) in Grenoble, France. The wavelengths used were 0.70135 and 0.69039 Å. The samples were contained in glass capillaries of 0.5 mm diameter. 2D images were collected with an exposure time of 10 s using a PILATUS image plate detector. The capillary was rotated 10° during the exposure. The 2D datasets were integrated into one-dimensional powder diffraction patterns with the program FIT2D [27]. PXD data were also obtained with a Bruker AXS D8 Advance diffractometer equipped with a Göbbel mirror and a LynxEye 1D strip detector. In this case, patterns were obtained in a Debye-Scherrer geometry using Cu Kα radiation (λ = 1.5418 Å) and rotating glass capillaries, filled and sealed under Ar atmosphere. The PXD data were analyzed using DIFFRAC.SUITE software (BRUKER) for phase identification. All PXD measurements were performed at R*T*.

Postprint.
Original in International Journal of Hydrogen Energy, Volume 41, Issue 23, 22 June 2016, Pages 9885–9892

Gravimetric desorption was performed using combined differential scanning calorimetry-thermogravimetric (DSC-TGA) instrument (Netzsch STA 449 F3 Jupiter). The samples were heated to the required *T* at heating rate of 10 K/min in a 50 mL/min Ar flow.

Attenuated total reflection Fourier transformed infrared (ATR FT-IR) spectra were collected with a Bruker Alpha-Platinum infrared spectrometer on a diamond crystal. The spectra were obtained in the range of 4000-400 cm^{-1} with a resolution of 2 cm^{-1}. The samples were measured without any dilution inside an argon-filled glove box. IR spectra were ATR-corrected using the commercial spectroscopic software OPUS.

Kinetics modeling

For the kinetics modeling, only the isothermal parts of desorption (and absorption) curves were considered. In case of desorption in vacuum, the reacted fraction, y ($y = \Delta wt/\Delta wt_{max}$), obtained during heating was neglected, thus $y = 0$ at the beginning of the isothermal step. Decomposition at all *T* and *p* was assumed to follow the same pathway. Therefore $y = 1$ was set at the maximum desorption wt% values obtained at 271-281 °C, i.e at 6.8 wt% for decomposition in vacuum. The isotherms were compared to the solid-state reaction models [25, 26], described in Table 2.

Table 2. Solid-state reaction models (general equation and the equation for y=0.5 at $t = t_{0.5}$) used for comparison with the experimental desorption and absorption curves [25, 26].

Short name	Equation	Description	Ref.
D1	$D_1(y) = y^2 = \frac{k}{x^2}t; D_1(0.5) = 0.2500\left(\frac{t}{t_{0.5}}\right)$	1-dimentional diffusion-controlled reaction with constant diffusion coefficient, where *2x* is the thickness of the reacting layer	[26]
D2	$D_2(y) = (1-y)\ln(1-y) + y = \frac{k}{r^2}t = 0.1534\left(\frac{t}{t_{0.5}}\right)$	2-dimentional diffusion-controlled reaction into a cylinder of radius *r*	[28]

D3	$D_3(y) = (1-(1-y)^{1/3})^2 = \frac{k}{r^2}t = 0.0426\left(\frac{t}{t_{0.5}}\right)$	3-dimentional diffusion-controlled reaction in a sphere of radius *r*	[29]
D4	$D_4(y) = \left(1-\frac{2y}{3}\right) - (1-y)^{2/3} = \frac{k}{r^2}t = 0.0367\left(\frac{t}{t_{0.5}}\right)$	Diffusion-controlled reaction starting on the exterior of a spherical particle of radius *r*	[30]
R2	$R_2(y) = 1-(1-y)^{1/2} = \frac{u}{r}t = 0.2929\left(\frac{t}{t_{0.5}}\right)$	Phase-boundary controlled reaction at the interface, for a circular disk reacting form the edge inwards, or for a cylinder, where *u* is a constant velocity of the interface	[26]
R3	$R_3(y) = 1-(1-y)^{1/3} = \frac{u}{r}t = 0.2063\left(\frac{t}{t_{0.5}}\right)$	Phase-boundary controlled reaction at the interface, for a sphere of radius *r*, reacting from the surface inward, where *u* is a constant velocity of the interface	[26]
A2	$A_2(y) = (-\ln(1-y))^{\frac{1}{2}} = kt = 0.8326t/t_{0.5}$	Avrami-Erove'ev equation for two dimensional growth of random nuclei with constant interface velocity	[31-34]
A3	$A_3(y) = (-\ln(1-y))^{\frac{1}{3}} = kt = 0.8850(t/t_{0.5})$	Avrami-Erove'ev equations for three dimensional growth of random nuclei with constant interface velocity	[31-34]

Results and Discussion

Desorption and absorption isotherms, and the reaction products

Decomposition reactions were carried out in Ar flow (gravimetric measurements, Figure 1a), initial static vacuum, and initial H_2 backpressure (p_0 (H_2) = 2.6 bar) (Figure 1b). In Ar flow, the decomposition at 265.0 and 285.0 °C yielded 8.1 and 9.1 Δwt%, respectively. The differences in weight loss can be explained by a slight temperature overshoot (till 297 °C) at the end of the heating ramp had triggered the next decomposition reaction step. This was confirmed by the PXD analysis of the reaction products (see below). In the volumetric measurements the partial decomposition at 260-285 °C yielded up to 6.8 wt% H_2 in vacuum. The amounts desorbed at H_2 backpressure were slightly lower. This can be explained by limited but non-negligible desorption during the heating step, despite the 50 bar H_2 pressure applied before the isothermal

Postprint.
Original in International Journal of Hydrogen Energy, Volume 41, Issue 23, 22 June 2016, Pages 9885–9892

step to suppress decomposition. The decomposition reactions at ~220 °C in vacuum and H_2 yielded significantly lower weight losses due to the slower reaction kinetics. It is worth noting that the gravimetric losses observed at the different desorption conditions are similar. Hence, in this work we can rule out any significant sublimation of $Mg(BH_4)_2$ as observed in [20].

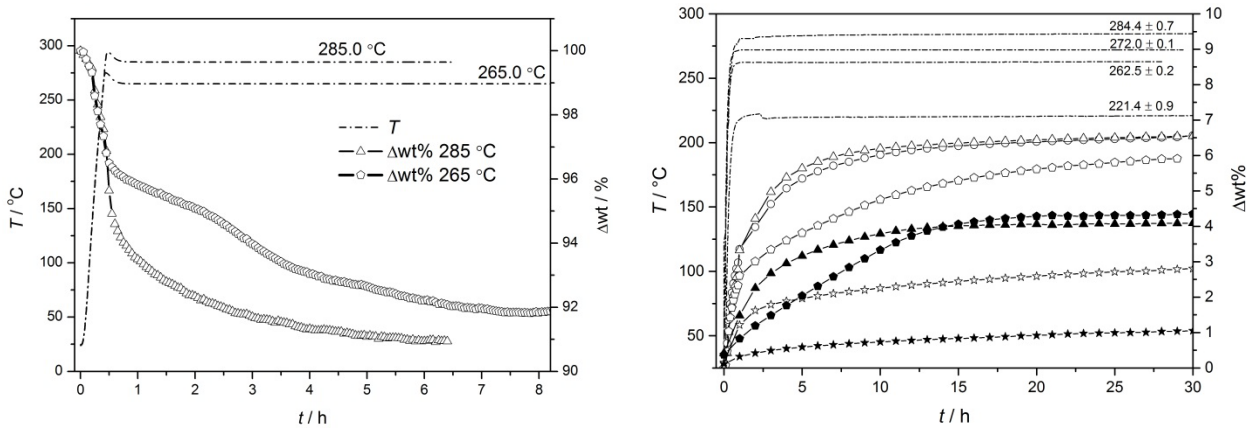

a) b)

Figure 1. Desorption curves for γ-$Mg(BH_4)_2$: a) TGA in Ar flow, b) volumetric measurements at p_0 = 0 (open symbols) and p_0 = 2.5 bar H_2 (filled symbols); triangles: 284 °C, circles: 272 °C, pentagons: 262-265 °C, stars: 221-222 °C. Dash-dot curves show the *T* curves for the measurements in vacuum with the T_{mean} ± SD of the isothermal step.

Rehydrogenation was carried out at 248.6, 260.3, and 279.8 °C, respectively (Figure 2). The reaction at 248.6 °C was particularly slow and the temperature was raised to 260.3 °C to complete it. The rehydrogenation curves show that 90% of the reaction was achieved within 3 to 8 hours at 279.8 and 260.3 °C, respectively. However, the total rechargeable capacity was 2.5 wt%, which is less than 40% of the maximum desorbed values. PXD and FTIR analysis of the rehydrogenation products showed amorphous $Mg_xB_yH_z$ phases in addition to crystalline β-and β′-$Mg(BH_4)_2$ (see the next section). It is known [14, 35, 36] that γ-$Mg(BH_4)_2$ undergoes phase transitions to eventually form β′-$Mg(BH_4)_2$ below 200 °C, and that rehydrogenation results in the formation of β- or β′-$Mg(BH_4)_2$ [19].

Postprint.
Original in International Journal of Hydrogen Energy, Volume 41, Issue 23, 22 June 2016, Pages 9885–9892

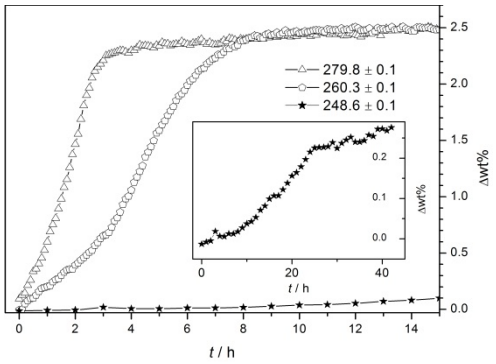

Figure 2. Absorption isotherms for partially decomposed $Mg(BH_4)_2$.

All the decomposition products were pale yellow to orange in color with the stronger tint of the samples decomposed at higher temperatures and in Ar, as reported earlier [14, 20]. After rehydrogenation the color of the samples paled to nearly white. Figure 3 shows PXD patterns (a,c) and the FTIR spectra (b,d) of the decomposition and rehydrogenation products. According to the PXD data, a significant and small amount of crystalline β-$Mg(BH_4)_2$ was observed after the decomposition at ~220 °C (both in vacuum and H_2) and at 265 °C in H_2, respectively, confirming the incomplete decomposition reactions. Decomposition at 284 °C yielded amorphous product(s), whereas the decomposition in Ar flow resulted in the formation of MgH_2. As suggested above, during the decomposition reactions in Ar, the temperature overshoot to 297 °C probably triggered the next decomposition step of the amorphous phases to the MgH_2, which explains also the slightly larger Δwt% H_2. Notably, this temperature for the MgH_2 formation is significantly lower than the temperature window of 330-365 °C reported in [35].

As for the rehydrogenation, at 279.8 °C and 120 bar H_2 (Figure 3c) the formation of β-$Mg(BH_4)_2$ [37] was observed. The pattern of the crystalline phase found after rehydrogenation at 260.3 °C resembled that of the intermediate β´-$Mg(BH_4)_2$ [14, 35, 36]. Note the formation of MgO in the desorption and absorption reactions, which might be a result of the presence of impurities in the starting material. Since no crystalline MgO was observed in the PXD pattern of the as-received γ-$Mg(BH_4)_2$, it can be suggested that some impurities might have been adsorbed in the pores of γ-$Mg(BH_4)_2$ (e.g oxygen) or, more likely, MgO could have originate from the

oxidized surface of γ-$Mg(BH_4)_2$. The presence of MgO could also be responsible for the incomplete rehydrogenation.

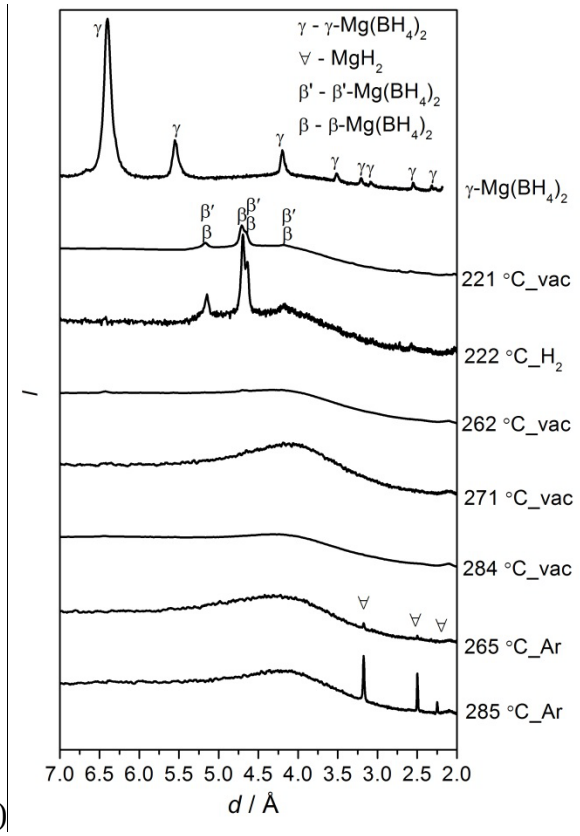

a)

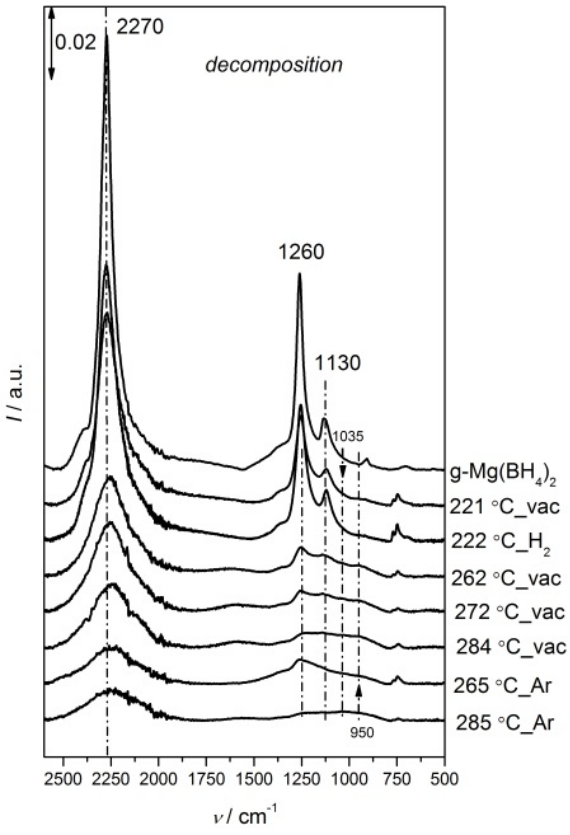

b)

Postprint.
Original in International Journal of Hydrogen Energy, Volume 41, Issue 23, 22 June 2016, Pages 9885–9892

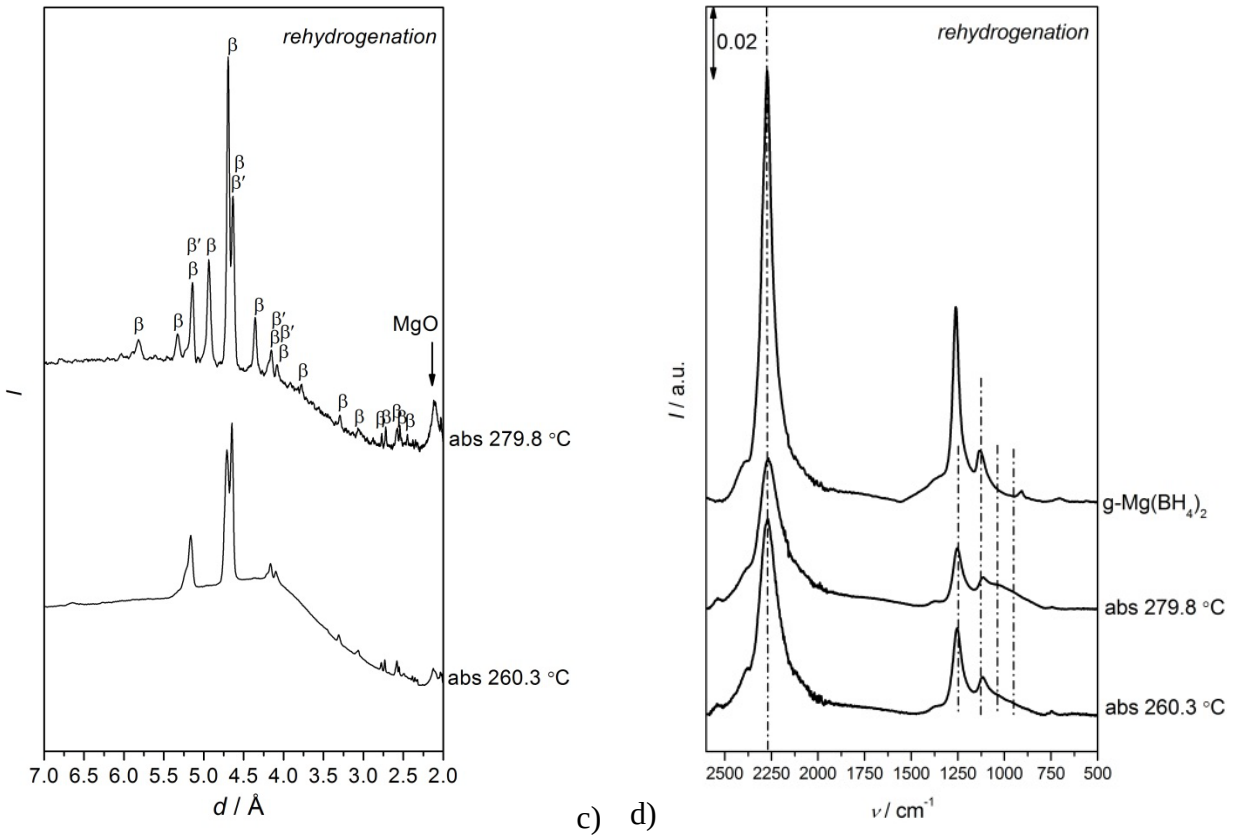

Figure 3. PXD patterns (a,c) and ATR-FTIR spectra (b,d) of γ-$Mg(BH_4)_2$ for the decomposition (a,b) and re-hydrogenation (c,d) reactions products. Intensity in the PXD patterns is normalized to the background at d = 7.0-6.8. Signal-to-intensity ratios of the PXD patterns are different due to different X-ray sources (synchrotron: samples des 221, 262, 284 °C, abs 279.8; and laboratory). The phases are marked according to the lit.: γ-$Mg(BH_4)_2$ [38], β-$Mg(BH_4)_2$ [37], β'-$Mg(BH_4)_2$ [14, 36]. The peaks at 2270, 1260, and 1130 cm^{-1} in the ATR-FTIR spectra are assigned to $Mg(BH_4)_2$.

FTIR spectra (Figure 3b) show the vibrations of the B-H-containing molecular groups in the amorphous and crystalline reaction products. Spectrum of the as-received $Mg(BH_4)_2$ shows IR absorption bands corresponding to the internal vibrations of BH_4^- ions [39]. The B–H fundamental stretching modes are centered at 2270 cm^{-1}, whereas the bending modes are located at *ca.* 1260 and 1130 cm^{-1}. Absorption due to the overtones and combinations of BH_4^- bending

are observed at 2390 cm^{-1}. The peaks at 913 and 706 cm^{-1} may be attributed to impurities, for example borates [40] that could have been responsible for the formation of MgO during the desorption and absorption. The IR spectra after desorption at all temperatures but 285 °C in Ar and vacuum still show the peaks corresponding to $Mg(BH_4)_2$ stretching and bending modes, such as the combination at 2270, 1260 and 1130 cm^{-1}. The intensities of these peaks have decreased with the increased dehydrogenation temperatures, as new peaks appear at ~1145, ~1035, ~950, 770, 747, and 695 cm^{-1}. The latter three peaks were shown to originate from the B-B ring breathing mode [20] and indicate that the dehydrogenated phase(s) should contain at least B_3 ring units. The corresponding B-H stretching modes are comprised within the broad absorption in the 2500-1900 cm^{-1} region. The IR spectrum of the sample decomposed in Ar flow and vacuum at 285 °C shows only the broad absorption in the BH stretching (2600-1800) and bending (1600-800 cm^{-1}) regions. Rehydrogenation resulted in an increase of the IR absorption intensities of $Mg(BH_4)_2$, and partial disappearance of the 770, 747, 695 peaks (Figure 3d), indicating their relation to the reversible phase.

Kinetics of the decomposition and rehydrogenation reactions

The experimental isotherms were compared to several theoretical models for solid-state reactions in order to investigate the reaction-limiting steps [25, 26]. The models were developed for simple one-step solid-state reactions but have also been extensively applied to the reactions in hydrides [41, 42]. Figure 4 shows the decomposition and rehydrogenation isotherms, plotted as the reacted fraction $y(t/t_{0.5})$, where $t_{0.5}$ corresponds to the time when $y = 0.5$. Decomposition reactions at ~220 °C did not reach y=0.5 and were not analyzed.

For $y < 0.5$ (insets on Figure 4 a,b), the desorption seems to be limited by diffusion and propagation of an interface (D1 to D4, R2 and R3 models), although it was difficult to distinguish between the different models. After $y > 0.5$ the distinction became more obvious, and diffusion seemed to be the prevalent rate-limiting step in all desorption curves except the decomposition at 262.5 °C in H_2. The latter most closely followed the phase-boundary-controlled model (R2 and R3). It appears thus that at the lowest temperature and H_2 back pressure chemical reactions(s) and diffusion through the interface limit the overall decomposition reaction kinetics.

Postprint.
Original in International Journal of Hydrogen Energy, Volume 41, Issue 23, 22 June 2016, Pages 9885–9892

It is worth noting that none of the desorption curves followed any particular model throughout all the desorption isotherms. Since none of the isotherms was found to follow strictly a particular reaction mechanism, it may be suggested that at the conditions applied in this work the decomposition is governed by a complex mechanisms consisting of several competing reactions. An attempt to determine the activation energy of the decomposition using the Arrhenius equation, for the isotherms at 262.5, 272.0, and 284.4 °C obtained in vacuum, was unsuccessful. This further suggests that the desorption reactions were not isokinetic over this temperature range. In addition, it is likely that the different reaction mechanisms results in different reaction products, which might be responsible for the incomplete rehydrogenation observed during absorption.

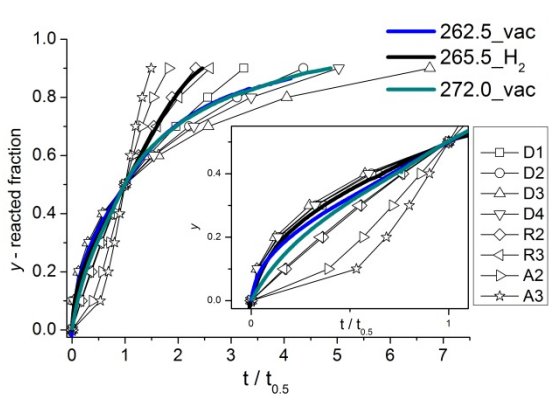

a)

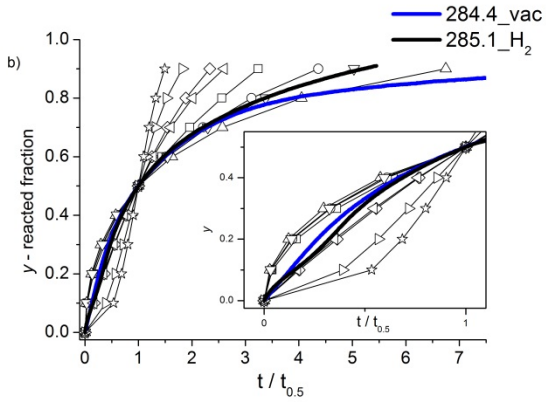

b)

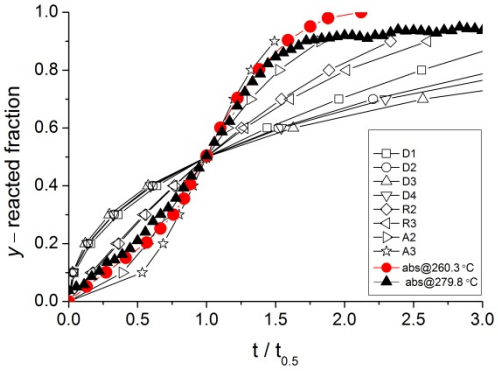

c)

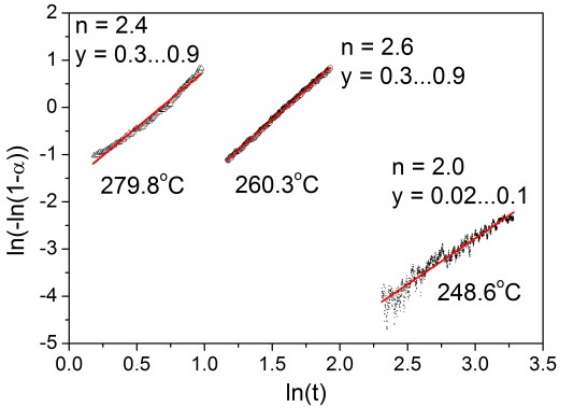

d)

Postprint.
Original in International Journal of Hydrogen Energy, Volume 41, Issue 23, 22 June 2016, Pages 9885–9892

Figure 4. Comparison of the desorption (a,b) and absorption (c) reactions to the solid state reaction models listed in Table 2 [25, 26]. The models were built using numerical data from ref. [26]. d) JMA plots for the absorption reactions, the reaction exponent *n* determining the limiting steps. The insets on the Figures a,b zoom in the region of the first reaction steps ($y < 0.5$). The models considered here are: D1, D2, and D3: 1-, 2-, and 3-dimensional diffusion-controlled reactions, respectively; D4: diffusion-controlled reaction starting on the exterior of a spherical particle; R2 and R3: inwards phase-boundary-controlled reactions for a circular disk or a cylinder (R2), and sphere (R3); A2 and A3: reactions controlled by nucleation and/or growth following Avrami-Erofe'ev equations (see also (Table 2)).

The absorption reactions (Figure 4c) most convincingly resembled Avrami-Erofe'ev models for nucleation and growth-controlled mechanisms. The linear fitting of $\ln(-\ln(1-y))$ vs. $\ln(t)$ curves resulted in an Avrami exponent *n* of 2.4-2.6 which corresponds to nucleation at a constant rate and diffusion-controlled growth mechanism. The attempt to apply the JMA modeling to the 248.6 °C isotherm in vacuum, taking 2.5 wt% as $y = 1$, yielded in the $n = 2$, corresponding to the diffusion-controlled growth of disks of constant thickness. However, modeling of the 248.6 °C reaction comprised the very initial reaction stages when $y = 0.02$-0.1.

Earlier it was suggested [43] that at 200 °C $Mg(BH_4)_2$ undergoes reversible rehydrogenation to the triborane $Mg(B_3H_8)_2$ according to eq. (1) and yielding 2.5 wt% of H_2:

$$3Mg(BH_4)_2 \leftrightarrow Mg(B_3H_8)_2 + 2MgH_2 + 2H_2 \qquad \text{eq. 1}$$

Another decomposition pathway [20] foresees 3.7 wt% H_2 release as shown below in eq. 2:

$$2Mg(BH_4)_2 \rightarrow MgB_4H_{10} + MgH_2 + 2H_2 \qquad \text{eq. 2}$$

Note that below 285 °C we have not found any crystalline MgH_2 after dehydrogenation, as predicted by eq. 1 and 2. The PXD patterns did not even exhibit the broad diffraction halos that could account for nano-crystalline MgH_2. Also the IR spectra have not given clear evidence for the bridged B-H-B vibrations expected from $(B_3H_8)^{2-}$ ions. However, the IR absorptions at 770, 747, and 695 cm^{-1} (Figure 3b,d), which seem to belong to the reversible phase, match those assigned to the $(B_4H_{10})^{2-}$ in [20] by comparing the calculated spectra of various B_yH_z anions.

According to those calculations, $(B_4H_{10})^{2-}$ does not have the pronounced IR features due to the B-H-B stretching which is in fair agreement with our IR analysis.

Our desorption values of up to 6.8 wt% H_2 in static vacuum are significantly higher than those suggested by the above eq. 1 and 2. Such weight loss would correspond to an overall reaction described by eq.3, assuming no loss in boron via release of B_2H_6 [44]:

$$Mg(BH_4)_2 \rightarrow \text{“}MgB_2H_{4.3}\text{”} + 1.8H_2 \qquad \text{eq. 3}$$

where “$MgB_2H_{4.3}$” is not a compound but accounts for the mixture of the reaction products, one of them possibly being MgB_4H_{10} [20]. The stoichiometric release of B_2H_6 is improbable because one B_2H_6 molecule accounts for 50 wt% of the $Mg(BH_4)_2$ weight. It is worth stressing that the mixture of reaction products in eq. 3 does not include MgH_2, as our PXD data strongly indicate. MgH_2 was only found when the samples were heated above 280 °C in Ar and a 9.1 wt% loss was observed. Thus it forms only during the next decomposition step.

It is rather puzzling that it was possible to re-absorb only about 2.5 H_2 wt%, or only 40% of the desorbed amount. The above discussion suggests that during desorption at least two Mg-B-H phases are formed, only one of which being reversible to $Mg(BH_4)_2$, and could explain the limited absorption. Another boron-containing intermediate compound forming in this partial decomposition reaction can be too stable and prevent the complete re-hydrogenation. However, the formation of MgO at the expenses of $Mg(BH_4)_2$ might have also been responsible for the reduced reversibility. For example, MgO could have possibly formed a shell around the reversible $Mg_xB_yH_z$ phases preventing the full rehydrogenation to $Mg(BH_4)_2$.

Conclusions

The partial decomposition reaction in $Mg(BH_4)_2$ in vacuum, hydrogen back pressure, and Ar was studied. Prior to the formation of MgH_2 above 280 °C, $Mg(BH_4)_2$ decomposed to $Mg_xB_yH_z$ amorphous reaction products with up to 6.8 wt% loss and following the overall reaction $Mg(BH_4)_2 \rightarrow$ “$MgB_2H_{4.3}$” + $1.8H_2$. It was possible to re-absorb only 40% of the desorbed capacity with the formation of different crystalline phases of $Mg(BH_4)_2$. The incomplete rehydrogenation might be due to the formation of several decomposition products, only some of them being reversible back to $Mg(BH_4)_2$. The formation of MgO may also be

Postprint.
Original in International Journal of Hydrogen Energy, Volume 41, Issue 23, 22 June 2016, Pages 9885–9892

responsible for incomplete rehydrogenation. Kinetics modeling showed that the desorption reactions could not be adequately described throughout the entire pathway by the solid-state reaction models considered in this work. However the modeling indicated diffusion as the most probable rate-limiting step in the reactions. Rehydrogenation clearly followed nucleation at a constant rate and a diffusion-controlled growth reaction mechanisms. It can then be suggested that the experimental approaches aimed at enhancing the bulk diffusion can improve the kinetics of the partial decomposition reaction in $Mg(BH_4)_2$. Besides overcoming the diffusion limitations, it should be possible to enhance the rehydrogenation by introducing phases that act as nucleation centers for the formation of crystalline $Mg(BH_4)_2$.

Highlights

- $Mg(BH_4)_2$ releases up to 6.8 wt% H_2 in the intermediate decomposition reaction to amorphous $Mg_xB_yH_z$ compounds.
- Rehydrogenation at T < 285°C and 120 bar H_2 yields in 2.5 wt% uptake and crystalline $Mg(BH_4)_2$.
- Kinetics modeling suggests that the desorption reaction(s) follow a complex pathway with different limiting steps.
- Rehydrogenation reaction(s) are governed by nucleation at a constant rate and diffusion-controlled growth.

Acknowledgements

This work was financed by the European Fuel Cells and Hydrogen Joint Undertaking (http://www.fch-ju.eu) under collaborative project “BOR4STORE” (Grant agreement no.: N° 303428). Part of this work was carried out at the Swiss-Norwegian beam-line of the European Synchrotron Radiation facility (ESRF-SNBL, BM01A). The skillful assistance of the beam line personnel at is gratefully acknowledged

References

Postprint.
Original in International Journal of Hydrogen Energy, Volume 41, Issue 23, 22 June 2016, Pages 9885–9892

[1] Hirscher M. Handbook of hydrogen storage new materials for future energy storage: Weinheim Wiley-VCH-Verl 2010.
[2] Sakintuna B, Lamari-Darkrim F, Hirscher M. Metal hydride materials for solid hydrogen storage: A review. Int J Hydrogen Energy. 2007;32:1121-40.
[3] Graetz J. New approaches to hydrogen storage. Chem Soc Rev. 2009;38:73-82.
[4] Li H-W, Yan Y, Orimo S, Züttel A, Jensen CM. Recent Progress in Metal Borohydrides for Hydrogen Storage. Energies. 2011;4:185-214.
[5] Solid hydrogen storage, http://www.mcphy.com/en/products/solid-hydrogen-storage/, Last accessed 15.11.2015.
[6] Hydrexia's Patented Hydrogen Storage Technology, http://hydrexia.com/hydrexia-hydrogen-storage-technology/, Last accessed on 15.11. 2015.
[7] Energy OoEEaR. Hydrogen Storage, http://energy.gov/eere/fuelcells/hydrogen-storage, Last accessed on 15.11.2015.
[8] Ozolins V, Majzoub EH, Wolverton C. First-principles prediction of a ground state crystal structure of magnesium borohydride. Phys Rev Lett. 2008;100:135501(1)-(4).
[9] Ozolins V, Majzoub EH, Wolverton C. First-Principles Prediction of Thermodynamically Reversible Hydrogen Storage Reactions in the Li-Mg-Ca-B-H System. J Am Chem Soc. 2009;131:230-7.
[10] van Setten MJ, de Wijs GA, Fichtner M, Brocks G. A density functional study of alpha-Mg(BH(4))(2). Chem Mater. 2008;20:4952-6.
[11] Chong M, Karkamkar A, Autrey T, Orimo S-i, Jalisatgi S, Jensen CM. Reversible dehydrogenation of magnesium borohydride to magnesium triborane in the solid state under moderate conditions. Chem Commun. 2011;47:1330-2.
[12] Hanada N, Chlopek K, Frommen C, Lohstroh W, Fichtner M. Thermal decomposition of Mg(BH4)2 under He flow and H2 pressure. J Mater Chem. 2008;18:2611-4.

Postprint.
Original in International Journal of Hydrogen Energy, Volume 41, Issue 23, 22 June 2016, Pages 9885–9892

[13] Li HW, Kikuchi K, Nakamori Y, Ohba N, Miwa K, Towata S, et al. Dehydriding and rehydriding processes of well-crystallized Mg(BH4)2 accompanying with formation of intermediate compounds. Acta Mater. 2008;56:1342-7.
[14] Paskevicius M, Pitt MP, Webb CJ, Sheppard DA, Filso U, Gray EM, et al. In-Situ X-ray Diffraction Study of gamma-Mg(BH4)(2) Decomposition. J Phys Chem C. 2012;116:15231-40.
[15] Riktor MD, Sørby MH, Chlopek K, Fichtner M, Buchter F, Züttel A, et al. In situ synchrotron diffraction studies of phase transitions and thermal decomposition of Mg(BH4)(2) and Ca(BH4)(2). J Mater Chem. 2007;17:4939-42.
[16] Saldan I, Frommen C, Llamas-Jansa I, Kalantzopoulos GN, Hino S, Arstad B, et al. Hydrogen storage properties of gamma-Mg(BH4)(2) modified by MoO3 and TiO2. Int J Hydrogen Energy. 2015;40:12286-93.
[17] Saldan I, Hino S, Humphries TD, Zavorotynska O, Chong M, Jensen CM, et al. Structural changes observed during the reversible hydrogenation of Mg(BH4)2 with Ni-based additives. J Phys Chem C. 2014;118:23376-84.
[18] Soloveichik GL, Gao Y, Rijssenbeek J, Andrus M, Kniajanski S, Bowman RC, Jr., et al. Magnesium borohydride as a hydrogen storage material: Properties and dehydrogenation pathway of unsolvated Mg(BH4)(2). Int J Hydrogen Energy. 2009;34:916-28.
[19] Zavorotynska O, Saldan I, Hino S, Humphries TD, Deledda S, Hauback BC. Hydrogen cycling in gamma-Mg(BH4)(2) with cobalt-based additives. J. Mater Chem. A. 2015;3:6592-602.
[20] Vitillo JG, Bordiga S, Baricco M. Spectroscopic and Structural Characterization of Thermal Decomposition of γ-Mg(BH4)2: Dynamic Vacuum vs. H2 Atmosphere. J Phys Chem C. 2015.
[21] van Setten MJ, Lohstroh W, Fichtner M. A new phase in the decomposition of Mg(BH4)(2): first-principles simulated annealing. J Mater Chem. 2009;19:7081-7.
[22] Newhouse RJ, Stavila V, Hwang S-J, Klebanoff LE, Zhang JZ. Reversibility and Improved Hydrogen Release of Magnesium Borohydride. J Phys Chem C. 2010;114:5224-32.
[23] Rönnebro E. Development of group II borohydrides as hydrogen storage materials. Curr Opin Solid State Mater Sci. 2011;15:44-51.

Postprint.
Original in International Journal of Hydrogen Energy, Volume 41, Issue 23, 22 June 2016, Pages 9885–9892

[24] Li H-W, Kikuchi K, Sato T, Nakamori Y, Ohba N, Aoki M, et al. Synthesis and Hydrogen Storage Properties of a Single-Phase Magnesium Borohydride Mg(BH4)(2). Mater Trans, JIM. 2008;49:2224-8.
[25] Gross KJ, Carrington RK, Barcelo S, Karkamkar A, Purewal J, Ma S, et al. Recommended Best Practices for the Characterization of Storage Properties of Hydrogen Storage Materials, US Department of Energy; http://energy.gov/eere/fuelcells/downloads/recommended-best-practices-characterization-storage-properties-hydrogen-0; 2012. p. 579, last accessed 15.11.2015.
[26] Sharp JH, Brindely GW, Narahari Achar BN. Numerical Data for Some commonly Used Solid State Reaction Equations. J Am Ceram Soc. 1966;49:379-82.
[27] Hammersley AP. FIT2D: An Introduction and Overview. ESRF Internal Report. 1997;ESRF97HA02T.
[28] Holt JB, Cutler IB, Wadsworth ME. Rate of Thermal Dehydration of Kaolinite in Vacuum. J Am Ceram Soc. 1962;45:133-6.
[29] Jander W. Reactions in solid states at room temperature I Announcement the rate of reaction in endothermic conversions. Z Anorg Allg Chem. 1927;163:1-30.
[30] Ginstling AM, Brounshtein BI. Concerning the Diffusion Kinetics of Reactions in Spherical Particles Zh Prikl Khim. 1950;23:1249-59.
[31] Avrami M. Kinetics of phase change I - General theory. J Chem Phys. 1939;7:1103-12.
[32] Avrami M. Kinetics of phase change II - Transformation-Time Relations for Random Distribution of Nuclei. J Chem Phys. 1940;8:212-24.
[33] Avrami M. Granulation, Phase Change, and Microstructure - Kinetics of Phase Change. III. J Chem Phys. 1941;9:177-84.
[34] Erofe'ev BV. Generalized equation of chemical kinetics and its application in reactions involving solids. Cont Rend Acad Sci URSS. 1946;52:511-14.
[35] David WIF, Callear SK, Jones MO, Aeberhard PC, Culligan SD, Pohl AH, et al. The structure, thermal properties and phase transformations of the cubic polymorph of magnesium tetrahydroborate. PCCP. 2012;14:11800-7.

Postprint.
Original in International Journal of Hydrogen Energy, Volume 41, Issue 23, 22 June 2016, Pages 9885–9892

[36] Zavorotynska O, Deledda S, Vitillo J, Saldan I, Guzik M, Baricco M, et al. Combined X-ray and Raman Studies on the Effect of Cobalt Additives on the Decomposition of Magnesium Borohydride. Energies. 2015;8:9173.
[37] Her J-H, Stephens PW, Gao Y, Soloveichik GL, Rijssenbeek J, Andrus M, et al. Structure of unsolvated magnesium borohydride Mg(BH4)(2). Acta Crystallogr Sect B: Struct Sci. 2007;63:561-8.
[38] Filinchuk Y, Richter B, Jensen TR, Dmitriev V, Chernyshov D, Hagemann H. Porous and Dense Magnesium Borohydride Frameworks: Synthesis, Stability, and Reversible Absorption of Guest Species. Angewandte Chemie-International Edition. 2011;50:11162-6.
[39] Giannasi A, Colognesi D, Ulivi L, Zoppi M, Ramirez-Cuesta AJ, Bardaji EG, et al. High Resolution Raman and Neutron Investigation of Mg(BH4)(2) in an Extensive Temperature Range. J Phys Chem A. 2010;114:2788-93.
[40] Li J, Xia S, Gao S. FT-IR and Raman spectroscopic study of hydrated borates. Spectrochim Acta. 1995;51A:519-32.
[41] Chaudhary A-L, Sheppard DA, Paskevicius M, Pistidda C, Dornheim M, Buckley CE. Reaction kinetic behaviour with relation to crystallite/grain size dependency in the Mg–Si–H system. Acta Mater. 2015;95:244-53.
[42] Riktor MD, Deledda S, Herrich M, Gutfleisch O, Fjellvåg H, Hauback BC. Hydride formation in ball-milled and cryomilled Mg-Fe powder mixtures. Materials Science and Engineering B -Advanced Functional Solid-State Materials. 2009;158:19-25.
[43] Chong M, Karkamkar A, Autrey T, Orimo S, Jalisatgi S, Jensen CM. Reversible dehydrogenation of magnesium borohydride to magnesium triborane in the solid state under moderate conditions. Chem Commun. 2011;47:1330-2.
[44] Stadie NP, Callini E, Richter B, Jensen TR, Borgschulte A, Züttel A. Supercritical N-2 Processing as a Route to the Clean Dehydrogenation of Porous Mg(BH4)(2). J Am Chem Soc. 2014;136:8181-4.

Postprint.
Original in International Journal of Hydrogen Energy, Volume 41, Issue 23, 22 June 2016, Pages 9885–9892